Cellular/Molecular

Multivesicular Release Differentiates the Reliability of Synaptic Transmission between the Visual Cortex and the Somatosensory Cortex

Chao-Hua Huang, Jin Bao, and Takeshi Sakaba
Independent Junior Research Group Biophysics of Synaptic Transmission, Max Planck Institute for Biophysical Chemistry, 37077, Goettingen, Germany

Neurons in layer 4 (L4) of the cortex play an important role in transferring signals from thalamus to other layers of the cortex. Understanding the fundamental properties of synaptic transmission between L4 neurons helps us gain a clear picture of how the neuronal network in L4 cooperates to process sensory information. In the present study, we have determined the underlying parameters that govern synaptic strength, such as quantal size, size of readily releasable vesicle pool, and release probability (Pr) of excitatory synaptic connections within L4 of the visual cortex (V1) and the somatosensory cortex (S1) in mice. Although only a single vesicle is released per release site under physiological conditions at V1 synapses, multivesicular release (MVR) is observed at S1 synapses. In addition, we observed a saturation of postsynaptic receptors at S1 synapses. Other synaptic properties are similar in both cortices. Dynamic clamp experiments suggest that higher Pr and MVR at S1 synapses lower the requirement of the number of synaptic inputs to generate postsynaptic action potentials. In addition, the slower decay of synaptic current and the intrinsic membrane properties of the postsynaptic neuron also contribute to the reliable transmission between S1 neurons.

Introduction

Synaptic strength is determined by both presynaptic and postsynaptic factors. Three parameters, the number of releasable units, release probability (Pr), and the quantal size (q), set synaptic strength (Del Castillo and Katz, 1954). Changes in these parameters lead to alterations in synaptic strength, which result in short- and long-term synaptic plasticity (Thomson, 2000; Zucker and Regehr, 2002). Based on the manner in which synaptic vesicles are released upon a single nerve impulse, two distinct hypotheses of the release process were proposed. The first hypothesis, so-called "one-site, one-vesicle," suggests that only one vesicle can be released at one site after one action potential (AP) (Korn et al., 1981; Gulyás et al., 1993; Buhl et al., 1997; Egger et al., 1999; Feldmeyer et al., 1999; Silver et al., 2003; Murphy et al., 2004; Biró et al., 2005). Based on this model, changes in synaptic strength are all or none and the rate of vesicular replenishment following a release event becomes crucial for a steady-state rate of neurotransmission (Stevens and Wang, 1995; Dobrunz and Stevens, 1997). The alternate hypothesis, multivesicular release (MVR), provides more flexibility by allowing variations in the number of vesicles released (Tong and Jahr, 1994; Wadiche and Jahr, 2001; Oertner et al., 2002; Watanabe et al., 2005; Li et al., 2009). However, the existence of MVR, particularly at cortical synapses, remains controversial. Variability of synaptic responses is further determined by postsynaptic receptor properties such as saturation and desensitization, which reduce fluctuations of synaptic response, and changes synaptic reliability (Trussell et al., 1993; Foster et al., 2002; Harrison and Jahr, 2003).

Short-term plasticity is important for signal transmission in the sensory pathway because the time scale of incoming sensory signals is similar to that of short-term plasticity (Abbott et al., 1997; Zucker and Regehr, 2002; Cook et al., 2003; Abbott and Regehr, 2004). To understand how sensory information is processed in the cortex, it is necessary to investigate the synaptic properties of cortical synapses. In this study, we determined the quantal properties of excitatory connections between regular-spiking (RS) neurons in layer 4 (L4) of visual cortex (V1) and somatosensory cortex (S1) quantitatively. This connection is known as a model system of cortical synaptic transmission, as previously described (Stern et al., 1992; Feldmeyer et al., 1999; Petersen, 2002). These neurons in L4 receive signals from the thalamus and further transmit them to other layers in the cortex. At the same time, synaptic interactions between RS neurons often connect to each other within a short distance, which allows good voltage clamp (Lübke et al., 2000; Petersen and Sakmann, 2000; Lefort et al., 2009). We characterized the basic properties of cortical synapses in two major cortical regions. By comparing these properties, we addressed the issue of synaptic heterogeneity among different cortical regions. Furthermore, dynamic clamp experiments revealed the importance of such heterogeneity at synaptic level for the reliability of transmission between neurons.

Materials and Methods

Slice preparation. Coronal slices (300 μm) were prepared from the visual cortex of postnatal day (P)22–P28 NMRI mice with a vibrating mic-

Received May 10, 2010; revised July 15, 2010; accepted July 20, 2010.

C.H.H. is supported by Boehringer Ingelheim Fonds. We thank Erwin Neher, Tobias Moser, Oliver Schlüter, and Raunak Sinha for discussion and comments on the manuscript.

Correspondence should be addressed to either Chao-Hua Huang or Takeshi Sakaba, Independent Junior Research Group Biophysics of Synaptic Transmission, Max Planck Institute for Biophysical Chemistry, Am Fassberg 11, 37077, Goettingen, Germany. E-mail: chuang@gwdg.de or tsakaba@gwdg.de.

DOI:10.1523/JNEUROSCI.2381-10.2010

 0270-6474/10/3011994-11$15.00/0

rotome (VT1000/S1200S; Leica). For somatosensory cortex, brain slices (300 μm) were prepared from P19–P24 mice (Agmon and Connors, 1991). The slicing solution contained the following (in mM): 125 NaCl, 2.5 KCl, 25 $NaHCO_3$, 1.25 NaH_2PO_4, 3 $MgCl_2$, 0.1 $CaCl_2$, 0.4 L-ascorbic acid, 3 *myo*-inositol, 2 pyruvate, and 25 glucose. Before slicing, the slicing solution was frozen till it was half ice and half liquid, and then bubbled with 95% O_2/5% CO_2. For animals older than P26 (for visual cortex) and for those older than P23 (for somatosensory cortex), a sucrose solution was used for slicing instead of normal slicing solution. The sucrose solution contained the following (in mM): 60 NaCl, 2.5 KCl, 120 sucrose, 25 $NaHCO_3$, 1.25 NaH_2PO_4, 3 $MgCl_2$, 0.1 $CaCl_2$, 0.4 L-ascorbic acid, 3 *myo*-inositol, 2 pyruvate, and 25 glucose. After a brain slice was cut, it was transferred to a chamber with extracellular solution and incubated at 37°C for 1 h. During the incubation, the solution was constantly bubbled with 95%O_2/5%CO_2. The extracellular solution contained the following (in mM): 125 NaCl, 2.5 KCl, 25 $NaHCO_3$, 1.25 NaH_2PO_4, 1 $MgCl_2$, 2 $CaCl_2$, 0.4 L-ascorbic acid, 3 *myo*-inositol, 2 pyruvate, and 25 glucose. After incubation, the slices were stored in the same solution at room temperature and was bubbled with 95% O_2/5% CO_2.

Electrophysiology. L4 neurons can be recognized by their round shape and the small size of the somata (Stern et al., 1992; Feldmeyer et al., 1999). The relative location of those neurons in the six-layer structure of the cortex was carefully examined. Whole-cell voltage-clamp recordings were performed on the soma of L4 neurons. After a connected pair was identified, EPSCs under different conditions were recorded (EPC 10, HEKA) at a sampling rate of 50 kHz (filtered at 3–6 kHz). The resistance of glass pipettes we used was 3–5 MOhm, and the intracellular solution contained the following (in mM): 140 potassium gluconate, 20 KCl, 10 HEPES, 5 ATP-Mg, 5 phosphocreatine, and 0.5 GTP, and was adjusted to pH 7.2 with KOH. The osmolarity of this solution was ~330 mOsm. Liquid junction potential (~10 mV) was not corrected. Series resistances were all <20 MOhm, and 20–50% compensation was used. The data were further offline filtered with a low pass filter at 1 kHz before analysis. In some experiments, 50 μM D-AP5 (Tocris Bioscience) was applied, but NMDA receptors did not contribute to the peak EPSC amplitudes in our study (supplemental Fig. S1, available at www.jneurosci.org as supplemental material). To prevent saturation of postsynaptic AMPA receptors, 0.5 mM kynurenic acid (Tocris Bioscience) was added to extracellular solution in some experiments. In addition, in some experiments, 10 mM tetraethylammonium (TEA; Sigma) were applied to increase the releasing probability. In readily releasable pool (RRP)-depletion experiments, one half or two-thirds of the potassium gluconate were replaced with cesium gluconate, and 10 mM TEA were applied to block potassium channels and to prevent repolarization. Also, D-AP5 was always applied in this experiment. All experiments (except those in Figs. 1 and 2) were performed at 30–35°C.

Variance-mean analysis. Fifty hertz train stimulations were applied to a presynaptic neuron and EPSCs were recorded from a postsynaptic one. The stimulus train was applied every 10–20 s and was repeated more than 20 times. The data were excluded from analysis when rundown of the EPSCs was noticed. The amplitude of each EPSC was calculated from the average of five data points around the peak minus the baseline of each peak. The baseline was the average >50 points (1 ms) just before the onset of EPSCs. The stimulation was repeated over 20 times and the amplitude of each peak EPSC was taken for analysis. We averaged the EPSCs of each peak (first, second, third, and so on) over all stimuli and the mean and the variance were obtained. These two parameters of each peak were plotted against each other. The estimation of N, Pr, and q was done according to Scheuss and Neher (2001). Definition of N is the number of functional release sites or the vescicle number of RRP, which should be a fixed number. Pr refers to the combination of probability of vesicle occupancy at the slot and vesicular release probability, and q is the postsynaptic current amplitudes induced by a single vesicle release (Vere-Jones, 1966).

Deconvolution. The EPSCs were deconvolved with the mEPSC to estimate transmitter release rates (Van der Kloot, 1988; Diamond and Jahr, 1995). In practice, we used the same procedure as Neher and Sakaba (2001), except that no residual current component due to delayed clearance of glutamate was assumed. In each cell pair, the decay time constant of mEPSC was adjusted by varying the time constant until spontaneous events become delta-pulse-like events in the release rate trace. The mEPSC amplitudes were assumed to be 5 pA in the presence of 0.5 mM kynurenic acid (Kyn), which was verified by variance-mean analysis (supplemental information 5, available at www.jneurosci.org as supplemental material).

Dynamic clamp experiments. The simulated excitatory synaptic current was injected into the soma by a homemade hardware realization of dynamic clamp setup. It was composed of three stages, as follows: input signal filtering and conditioning (analog circuit), digitalization (AD7495; Analog Devices) and calculation (AT32AP7000; Atmel), and digital-to-analog conversion (DA5620; Analog Devices). The control program was written in C (with development environment AVR32 Studio 2.5.0 and compiler avr32-gcc 4.3.2). The simulated synaptic current, I, was calculated from the voltage-independent conductance, g, and the instantaneous driving force, $V - E$.

$$I = g \times (V - E). \quad (1)$$

V is the membrane potential measured from patch-clamp amplifier and fed to the dynamic clamp in each cycle. E is the reversal potential for AMPA receptors, which is set to 0 mV. g is modeled by a double exponential waveform

$$g = G \times (-\exp(-t/\tau_{rise}) + \exp(-t/\tau_{decay})). \quad (2)$$

G is a scaling factor for the peak amplitude. τ_{rise} and τ_{decay} were the time constants for the rising and decaying phases of the waveform and are taken to fit the recorded EPSCs. In each cycle of the dynamic clamp experiment, an updated I was calculated according to Equations 1 and 2 and fed to the soma through the patch pipette. For each simulated synaptic event, the peak amplitude of the conductance was a positive random number from a Gaussian distribution with the calculated mean and SD from recorded EPSC peak amplitudes (supplemental information 7, available at www.jneurosci.org as supplemental material). The updated rate of dynamic clamp was 50 kHz. Experiments were done in the presence of 10–25 μM bicuculine (Sigma).

Results

Variance-mean analysis and the mEPSC amplitude measurement at L4 neurons in V1

We performed simultaneous paired or triple recordings on the somata of L4 regular spiking neurons in mouse visual cortex. First, the neuronal type was identified according to the firing pattern of a neuron upon a current injection. These L4 neurons were then classified into three categories: RS neuron, fast spiking (FS) neuron, and low-threshold spiking neuron (LTS) (Fig. 1) (Buhl et al., 1997; Gupta et al., 2000; Beierlein et al., 2003). RS neurons form excitatory synapses onto the postsynaptic neuron, and FS and LTS neurons form inhibitory synapses. To test whether a pair of neurons was synaptically connected, we depolarized one of the two neurons from −80 to 0 mV for 2 ms to induce an action potential and examined whether we could record monosynaptic, time-locked responses from the other neuron and vice versa. Furthermore, to exclude disynaptic connections, only those connections in which the time difference between the onset of EPSCs and stimulation of the presynaptic neuron was restricted to <5 ms were selected for analysis. In this report, we focused on only RS–RS connections in L4.

After a connected pair was identified, 50 Hz train stimulations (depolarizations from −80 to 0 mV for 2 ms to induce an action potential) were applied to the presynaptic neuron and the EPSCs were recorded from the postsynaptic neuron. Figure 2*A* illustrates presynaptic and postsynaptic currents elicited by such stimulation under 2 mM extracellular Ca^{2+} at room temperature from a representative connection in V1. A train stimulation allowed us to sample EPSCs at different Pr within one trace. By

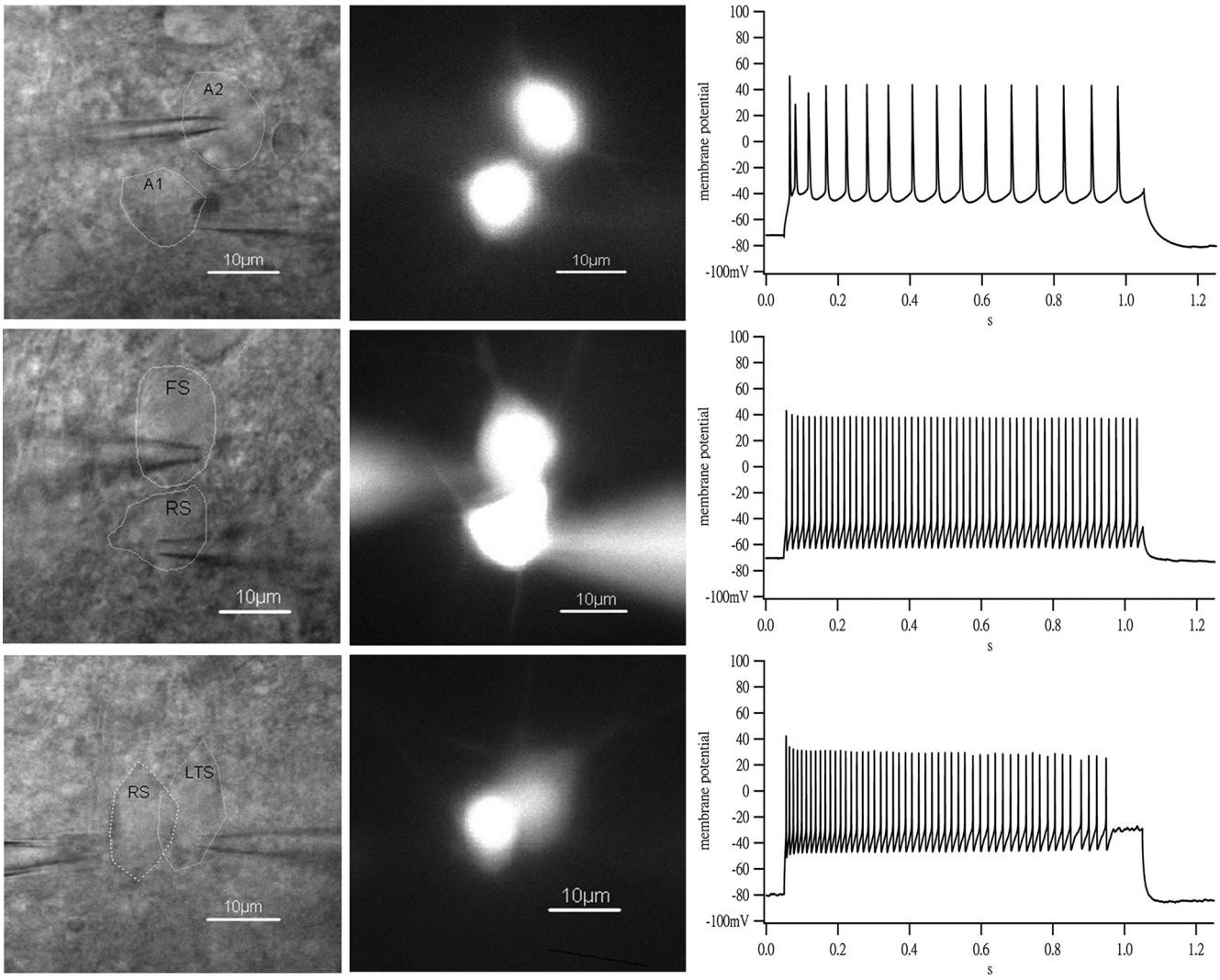

Figure 1. Three classes of excitatory connections in L4 of V1. The configuration of a paired recording from two neurons under bright field, and fluorescence images are shown (left and middle). The right panel shows the firing pattern of the postsynaptic neuron. Top, The connection between two RS neurons. The right panel shows the firing pattern of a RS neuron. Middle, The connection between a RS neuron and a FS neuron. The right panel shows the firing pattern of a FS neuron. Bottom, The connection between a RS and a LTS neuron. The right panel shows the firing pattern of a LTS neuron.

repeating this train stimulation with an interval of 10 s more than 20 times, the variance and mean of the EPSC amplitudes of each stimulus were obtained and variance-mean analysis (Scheuss and Neher, 2001; Silver, 2003) was performed to determine the synaptic parameters N, Pr, and q (see Material and Methods). Figure 2*A* shows that the relationship between variance and mean was linear. This indicates that Pr is low and only q could be obtained from this analysis. On average, the q estimated by variance-mean analysis was 9.2 ± 2.9 pA ($n = 3$, before corrected with a correction factor of 27%) [supplemental information 4, available at www.jneurosci.org as supplemental material, for coefficient of variation (CV) calculation]. We looked into the individual traces of each connection. As shown in Figure 2*B*, after the ninth stimulus, the EPSCs started to fluctuate in an all-or-none manner and the amplitudes of the success events remained the same, which might indicate that it resulted from release of a single vesicle. On the contrary, the amplitude of fifth EPSC exhibited considerable variability, indicating that more than one vesicle was released from the terminals at the fifth stimulus. We examined the EPSCs after the ninth stimulus in three connections, with a total of 49 individual events. The failure rate was >0.5 for each stimulus (when we pooled responses from all stimuli, the overall failure rate was >0.9), and the average amplitude of successful events was 9.3 ± 0.7 pA ($n = 49$). These amplitudes were consistent with those calculated from the variance-mean analysis, implying that the estimates from our method were valid.

To further confirm our results, we measured evoked mEPSCs and constructed an mEPSC amplitude histogram. For measuring evoked mEPSCs, the extracellular Ca^{2+} was reduced to 0.4–0.6 mM (Katz and Miledi, 1965; Isaacson and Walmsley, 1995), and the divalent cation concentration was kept constant by correspondingly increasing the concentration of Mg^{2+} to 3 mM. A 2 ms depolarization (from −80 to 0 mV) was applied repetitively to the presynaptic cell with an interval of 3 s, instead of 10–20 s, in this particular set of experiments, and the EPSCs were recorded from the postsynaptic cell. We calculated the failure rate in each connection and only the ones with a failure rate >0.5 were taken for further analysis. Overall, 126 mEPSC events were recorded from five connections, and the average failure rate was 0.6. The average mEPSC amplitude was 10.8 ± 0.48 pA. The distribution of mEPSC amplitudes were plotted together with the ones recorded from the train stimulation experiment in Figure 2*C*. The

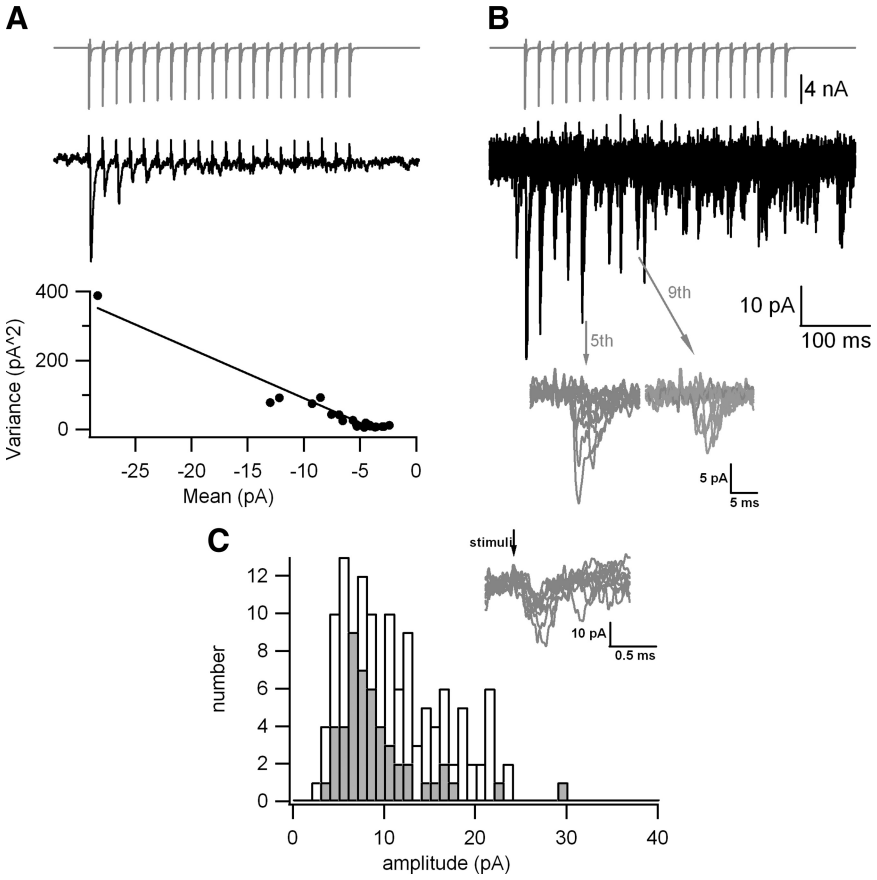

Figure 2. Variance-mean analysis predicts quantal sizes, which matches with the mEPSC amplitudes. ***A***, Top, Presynaptic current of a representative RS–RS connection in V1 upon a short depolarization at room temperature. Middle, Mean EPSC corresponding to the stimuli from the same connection. Bottom, Variance-mean relationship. Black solid circles represent the relationship of the variance and the mean of the EPSC amplitudes upon a stimulus train obtained from >20 repetitions. The line fit (black line) estimates q = 14.2 pA. ***B***, Individual EPSC traces from the same connection as ***A***. Ten individual traces of 20 repetitions are superimposed to show the fluctuation of EPSCs. The gray traces are the close look at individual peaks of the fifth and the ninth stimuli. ***C***, Histogram of the evoked mEPSCs obtained under low external Ca^{2+} (white bar). Inset, representative mEPSC traces under low Ca^{2+}. Gray bars indicate the histogram of mEPSCs obtained from train stimulation experiments.

amplitude distribution of mEPSC measurement was slightly skewed to the right and had a CV of 0.52. The histogram of these two methods (evoked mEPSCs and EPSC events during the late period in the train) overlapped quite well. Also the average mEPSC amplitudes were similar and matched closely with quantal amplitudes estimated from the variance-mean analysis.

Estimation of N, Pr, and q under physiological condition with variance-mean analysis

To examine the quantal parameters under more physiological conditions, the recording temperature was raised to 30–32°C in the following experiments. We repeated the same 50 Hz train stimulation protocol on RS–RS connections in V1 and applied variance-mean analysis to the evoked EPSCs in a stimulus train. In Figure 3*A*, left, the relationship of variance and mean could be fitted with a parabola in some connections. This indicates that temperature raises Pr considerably. From the parabola fit, the q and N were estimated. The average q was 9.88 ± 1.09 pA ($n = 5$). Postsynaptic receptor saturation may have caused a parabolic relationship (Meyer et al., 2001; Foster and Regehr, 2004). Therefore, we applied 0.5 mM Kyn, a low affinity AMPA receptor antagonist (Diamond and Jahr, 1997; Wadiche and Jahr, 2001) to the brain slice. Result is shown in Figure 3*A*. With Kyn, the variance-mean relationship of EPSCs was linear in three connections (Fig. 3*A*, right) and was parabola in four (Fig. 3*A*, left) of seven connections. Assuming the difference of these two groups (linear vs parabola) resulted from different Pr, only the four examples with a parabola relationship could be used to calculate the N and the Pr. The average N was 7 ± 1.1 ($n = 4$) and the average Pr was 0.59 ± 0.05 ($n = 4$). However, the average Pr must be lower than 0.59 because of three linear cases ($\ll 0.5$). This indicates that the release probability is heterogeneous at V1.

Although in some cases the Pr was high enough to show a parabolic relationship, the fraction of linear ones in the population was high as well. Therefore, we attempted to increase the Pr so that we could increase the number of parabola cases, thus allowing us to estimate N. To achieve this goal, we first tried the conventional way of increasing Pr by elevating the extracellular Ca^{2+} concentration to 4 or 8 mM Ca^{2+}. However, we could not observe any augmentation of EPSCs with high Ca^{2+} (data not shown). One possible reason could be the surface-charge screening effect due to excess divalent cations. Hence, another method was tested, which was to apply 10 mM TEA, a K^+ channel blocker, along with 0.5 mM Kyn, which is a low affinity AMPA receptor antagonist, in the bath. TEA is known to broaden the action potential waveform and thus increase the Ca^{2+} flux, which as a result might increase the Pr at terminals with TEA. Because rundown of release was faster under TEA (possibly due to the increased Pr), it was difficult to perform variance-mean analysis under both control and in the presence of TEA. The result is shown in Figure 3*B*. The average Pr was elevated to 0.69 ± 0.03 ($n = 11$), which showed that TEA did increase Pr. However, for a fraction of cells, the linear relationship remained (6 of 17 connections). We pooled all parabola cases in both experiments (with Kyn only and with Kyn and TEA), assuming that the N should be intrinsically the same as that of other synapses, and the final estimate of N was 6.3 ± 1.0 ($n = 13$).

Depletion of the readily releasable pool and calculating release rates with the deconvolution method

To verify the results from variance-mean analysis, we performed experiments to deplete the RRP of synaptic vesicles and measured the actual number of released vesicles. Part of the potassium in the intracellular solution was replaced with cesium, a K^+ channel blocker, and the concentration ratio of Cs^+ to K^+ in the intracellular solution was 2:1. We did not replace all K^+ with Cs^+ because cells did not tolerate such an extreme condition at physiological temperature. After a connected pair was identified, 10 mM TEA was applied to the bath to further block potassium channels. Subsequently, 0.5 mM Kyn was also added to prevent postsynaptic receptor saturation. With application of both Cs^+ and external TEA, we aimed for a step-like long depolarization at

the terminal, similar to the original idea of Katz and Miledi (1967) at the squid giant synapse. As shown in Figure 4*A*, two 100 ms depolarizations were given to the presynaptic neuron with an interval of 200 ms, and the EPSCs were recorded from the postsynaptic neuron. The protocol was repeated several times with an interval of >10 s, allowing the cell to fully recover from the previous stimulus. The second depolarization was applied to ensure complete depletion of the RRP, which was achieved in seven cell pairs. Although a perfect voltage clamp of the presynaptic terminal was not expected, relatively short length of axons (Feldmeyer et al., 1999), together with Cs^+-mediated blocking of K^+ channels, may have helped to attain sufficient stimulation of the terminal. The N was then calculated by the deconvolution method (Van der Kloot, 1988; Diamond and Jahr, 1995). Figure 4*B* shows the cumulative trace of release from a representative connection. On average, the N was 8.3 ± 0.9 ($n = 7$). There was no significant difference between the results from variance-mean analysis and the depletion experiment (t test, $p = 0.13$). Therefore, we concluded that the estimated N was valid (the assumption above was fulfilled). The result also suggests that a strong depolarization does not recruit an additional pool of vesicles that are not used during an AP. The vesicle replenishment rate following the RRP depletion could be obtained from the cumulative trace. In V1, the time required to refill the whole RRP (T_{rec}) under high [Ca^{2+}] was 91.4 ± 15.5 ms ($n = 7$), which was estimated by fitting the cumulative release trace with an exponential (representing the RRP) and a linear line (representing the replenishment). One may expect to see more recovered responses during the second pulse (applied at a 200 ms interval), given that the replenishment rate is <100 ms. Possibly, the Ca^{2+}-dependent component of vesicle replenishment is accelerated during the pulse, but a drop in Ca^{2+} after the pulse would decrease the rate of replenishment (Dittman and Regehr, 1998; Wang and Kaczmarek, 1998; Hosoi et al., 2007).

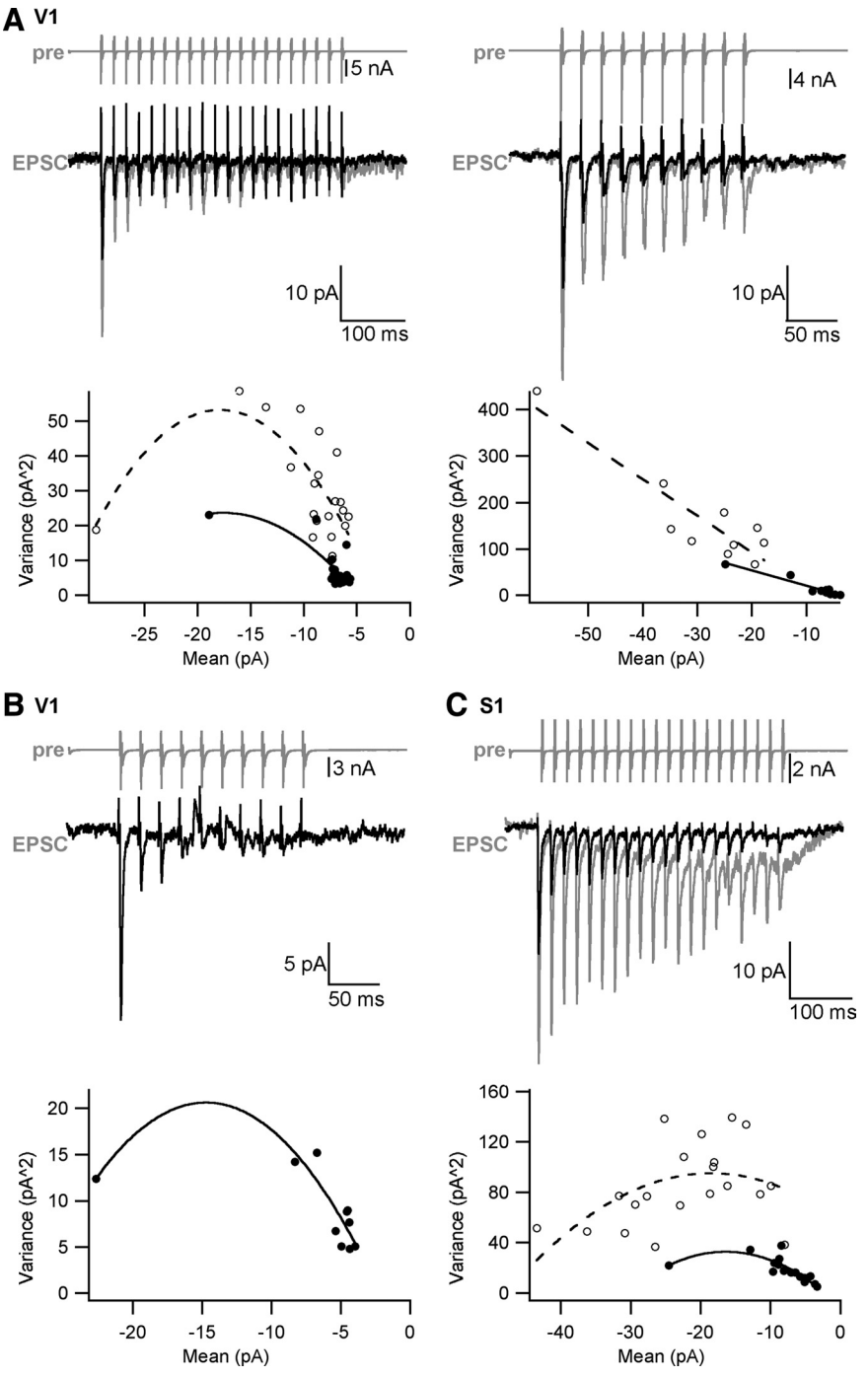

Figure 3. Estimation of N, Pr, and q under physiological condition with variance-mean analysis. ***A–C***, Top, Presynaptic currents of a representative RS–RS connection in V1 upon a short depolarization. Middle, Mean EPSCs in response to the stimuli from the same connection. The gray trace is the control group and the black one was obtained under 0.5 mM Kyn. Bottom, Variance-mean relationship of the EPSCs both in control (black hollow circles) and in the presence of Kyn (black solid circle). ***A***, Left, The parabola fit of the control (dashed line) estimates N = 4.2 and q = 8.7 pA. The fit of the group under Kyn (solid line) estimates N = 7 and q = 5 pA. Right, The linear fit of the control (dashed line) estimates q = 7.8 pA. The fit of the group under Kyn (solid line) estimates q = 3.3 pA. ***B***, Traces were obtained from the experiments with TEA and Kyn in V1. The parabola fit estimates N = 7.6 and q = 3.9 pA. ***C***, Traces from a representative RS–RS connection in S1. The parabola fit of the group with Kyn (black filled circles) estimates N = 6.25 and q = 5.3 pA.

Saturation of postsynaptic receptors at RS–RS connections in S1

From the data above, we have obtained the three important quantal parameters (N, Pr, and q) of RS–RS synapses in V1. The N of RS–RS connections in V1 was quite different from that determined in S1 synapses. According to Feldmeyer et al. (1999), the morphological synaptic contact number was three to four (Egger et al., 1999). Therefore, we examined whether the synaptic properties were different among different cortical areas. We repeated the variance-mean analysis and the depletion experiments at the RS–RS connections in the L4 of S1 at physiological temperature (30–35°C). The variance-mean analysis result is shown in Figure 3*C*. In the control group, the variance exhibited a shallow depen-

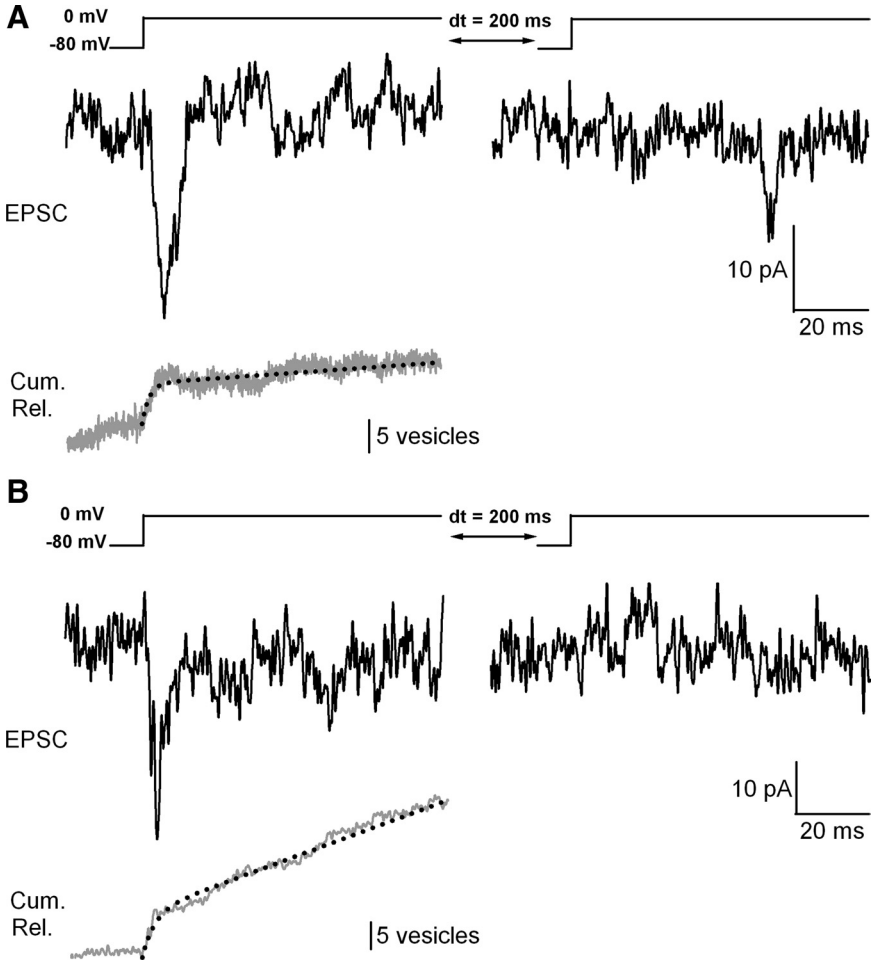

Figure 4. Depletion of the readily releasable pool and calculating cumulative release with deconvolution method. ***A***, A representative depletion trace from a representative RS–RS connection in V1. Top, Stimulation protocol. The presynaptic neuron was depolarized from −80 to 0 mV for 100 ms and, after an interval of 200 ms, the second 100 ms depolarization was applied to the cell to test the remaining vesicles within the RRP. Middle, One representative individual EPSC responding to a strong depolarization. Upon the second depolarization, there was no vesicle released, indicating depletion of the RRP. Bottom, Cumulative trace of release (Cum. Rel.) from deconvolution of the EPSC. The two components (an exponential and a line) fit is shown in the dashed line. From the fit, the number of vesicles in the RRP was estimated to be 7.4, the time constant of RRP depletion was 0.89 ms, and the vesicle replenishment rate constant was 70 ms in this case. ***B***, The order of panels is the same as ***A***, but ***B*** shows a representative trace from a representative RS–RS connection in S1. The cumulative trace of release was filtered at 1 kHz, so it is less noisy than that in ***A***, but this would not change the result. The fitting result shows that the number of vesicles within the RRP was 7.8, the time constant of RRP depletion was 3 ms, and the replenishment rate constant was 28 ms in this example.

dence on the mean. When a parabola was fitted to the data, the intercept of *x*-axis was far above 0. This indicates that the variance-mean analysis is not valid. It is possible that some postsynaptic factors, for example, saturation of the postsynaptic receptors (Foster and Regehr, 2004) distorted the relationship. To test this, we applied 0.5 mM Kyn to the slice and, as seen in Figure 3*C*, the variance-mean relationship was restored to parabola shape. Therefore, at RS–RS synapses in S1 postsynaptic receptor, saturation played a role during short-term synaptic plasticity. Under Kyn, the N in S1 was 7.4 ± 1.3 and the Pr was 0.66 ± 0.03 ($n = 9$). There was no significant difference between both values in S1 and those in V1 (*t* test; N, $p = 0.5$; Pr, $p = 0.27$). It is worthwhile to note that, in S1, all connections showed a parabola relationship under Kyn, whereas in V1, approximately half of the population was linear. Therefore, the overall Pr in V1 must be lower than S1 and more heterogeneous. Next, we performed the RRP depletion experiment to confirm the N from variance-mean analysis. The N was 8.1 ± 2.0 ($n = 7$), which was not significantly different from the value from variance-mean analysis (*t* test, $p = 0.77$). However, this number is much higher than previous estimates of the number of release sites at S1 (3 or 4; see Discussion) (Buhl et al., 1997; Feldmeyer et al., 1999). T_{rec} at high $[Ca^{2+}]$ in S1 was 34.3 ± 6.4 ms ($n = 7$). The summary of N, Pr, q, and T_{rec} of RS–RS synapses in both cortical areas is shown in Table 1.

A close look at the blocking effect of Kyn suggests multivesicular release in S1

As shown previously, Kyn restored the distorted variance-mean relationship of RS–RS connections in S1. Because differential block of Kyn is a strong indicator of MVR (Wadiche and Jahr, 2001), we looked into the blocking effect in more detail. Figure 5*A* illustrates the blocking efficiency of Kyn in both cortical areas. In the S1 group, the second and subsequent EPSCs were blocked significantly more than the first one, whereas there is no significant difference in V1. Even in the connections with high Pr, there was no differential block at V1. Differential block was not seen with NBQX (supplemental Fig. S2, available at www.jneurosci.org as supplemental material), a high affinity AMPA receptor antagonist, arguing against a voltage-clamp problem (Wadiche and Jahr, 2001). This result suggests that the local glutamate transient in the synaptic cleft changes during the train stimulation in active synapses in S1, but not in V1, under physiological condition. However, when TEA was applied to further increase Pr, a differential block of Kyn was also observed in V1 (supplemental Fig. S3, available at www.jneurosci.org as supplemental material). Though the effect is still less than in S1 under control condition, these data suggest that MVR could occur at RS–RS connections in V1 under high Pr but predominantly only one or no vesicle is released at a given site in the majority of the connections in V1 under physiological condition. The main reason for the low number of released vesicles is primarily due to a low Pr in V1 rather than some special transmitter release mechanism such as single vesicle constraint or lateral inhibition of release. We analyzed the blocking effect in an alternate way by plotting the depression curve of the train stimulation trace in Figure 5*B*. Here the EPSC amplitude was normalized to the first EPSC amplitude of each stimulus train. Again, in S1 the depression curve was significantly deeper under Kyn. Consistently, when we calculated paired-pulse ratio (PPR) of the first two EPSCs in a train, Kyn reduced the PPR at S1 but not at V1 (supplemental Fig. S6, available at www.jneurosci.org as supplemental material). These results, together with Figure 5, suggest that postsynaptic receptor saturation reduces the synaptic depression significantly, making the synapse more stable during the

Table 1. Summary of the synaptic parameters under different conditions

	q		N			T_{rec}	
	Variance-mean	Mini	Variance-mean	Pool depletion	Pr	Depression curve	Pool depletion
V1	9.2 ± 2.9 pA ($n = 3$, RT) 9.0 ± 0.9 pA ($n = 4$, PT)	10.8 ± 0.48 pA	7.0 ± 1.1 ($n = 4$, without TEA) 6.0 ± 1.3 ($n = 11$, with TEA)	8.3 ± 0.9 ($n = 7$)	<0.59 ± 0.05* ($n = 4$, without TEA) <0.69 ± 0.03* ($n = 11$, with TEA)	100 ms (Pr = 0.45)	91.4 ± 15.5 ms ($n = 7$)
S1			7.4 ± 1.3 ($n = 9$)	8.1 ± 2 ($n = 7$)	0.66 ± 0.03 ($n = 9$)	71 ms (Pr = 0.55)	34.3 ± 6.4 ms ($n = 7$)

q was obtained under control conditions, but variance-mean analysis did not work properly at S1. Under Kyn, qunatal sizes were estimated to be 5.5 ± 0.73 pA and 5.5 ± 0.7 pA in V1 and S1, respectively. Vesicle replenishment rates were estimated from the cumulative release trace in Fig 4 or from the depression curve during a 50 Hz train under Kyn (Fig 5). A simple vesicle pool depletion model (a single RRP with fixed replenishment rate) could explain the depression curve under Kyn, when the Pr was set to 0.55 and 0.45 and the replenishment rate was set to 71 ms and 100 ms in S1 and V1, respectively. RT, Room temperature; PT, physiological temperature.

*Considering that in V1, some connections did not show parabola relation in variance-mean analysis, the average Pr should be smaller than the value presented here in the table.

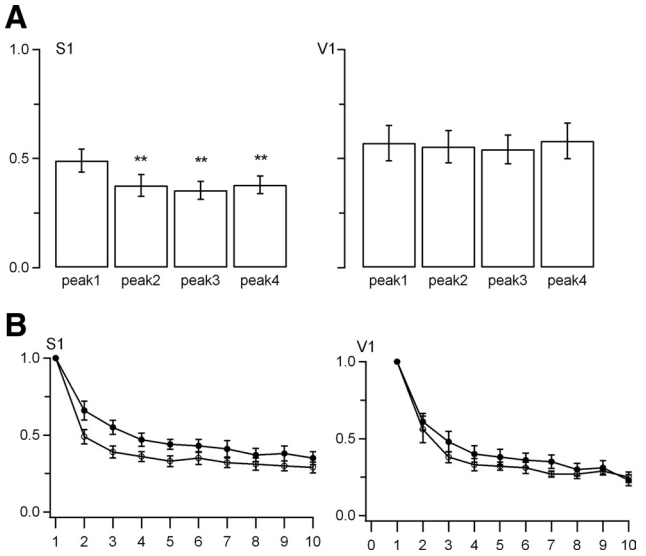

Figure 5. A close look at the blocking effect of 0.5 mM Kyn. ***A***, The remaining fraction of EPSC after blocking by Kyn. The EPSCs amplitude of each peak with Kyn was divided by that of the control group. The figure shows the average ratio of the first to the fourth peak over all connections we recorded. Left, Results from S1. There is a significant difference between the first peak and the rest (paired *t* test, first vs second, $p = 0.0007$; first vs third, $p = 0.0009$; first vs fourth, $p = 0.009$). The right panel shows the results from V1. There is no significant difference between the first peak and the rest (paired *t* test, first vs second, $p = 0.81$; first vs third, $p = 0.72$; first vs fourth, $p = 0.9$). ***B***, The depression curve of synaptic transmission is shown. The EPSCs of each stimulus are normalized to the first one. The filled circles represent the control group and the open circles represent the group under Kyn. Left, Results from S1. Right, Results from V1. In S1, there was significant difference (paired *t* test, $p < 0.05$) between control group and the condition under Kyn, whereas in V1 there was no significant difference (paired *t* test, $p > 0.1$) between the two groups.

train. However, V1 connections did not exhibit postsynaptic receptor saturation under the same condition.

S1 connections can induce a postsynaptic AP more reliably than V1 connections

The results above suggest that RS–RS connections in S1 are more reliable than those in V1. It remains to be tested how reliably a presynaptic AP can induce a postsynaptic AP. To test this issue, we first conducted simultaneous double-patch recordings and examined whether a presynaptic AP could induce a postsynaptic spike under current-clamp mode. However, whereas in both S1 and V1 only EPSPs were observed, no postsynaptic spikes were elicited upon a single AP (data not shown), in contrast with previous studies (Egger et al., 1999; Feldmeyer et al., 1999). This indicates that the input from a single neuron is not sufficient to trigger APs at a postsynaptic neuron; more inputs might be required for postsynaptic firing. Due to the technical difficulty of conventional electrophysiology, only a limited number of cells can be patched at the same time, so instead we performed dynamic clamp (Prinz et al., 2004) to systematically change the number of presynaptic neurons. Dynamic clamp is different from voltage clamp and current clamp because instead of clamping the membrane potential or current, conductance is applied to the cell and the amount of current flow depends on the instantaneous membrane potential. In our case, this method has the advantage that a postsynaptic neuron can be excited by virtual presynaptic inputs, which therefore precludes the need to patch several presynaptic neurons at the same time and hence test the reliability of producing spikes at the postsynaptic neuron. To mimic the real conductance change at a postsynaptic neuron upon an AP at a presynaptic neuron, the EPSCs measured at the soma of the postsynaptic neuron in the previous sets of experiments were used for the waveform of a unitary synaptic conductance and in calculating the mean peak amplitude and its variance (supplemental information 7, available at www.jneurosci.org as supplemental material). We assumed that multiple inputs are a linear summation of the unitary synaptic conductance and that they all arrive at the soma at the same time. This assumption may be overly simplistic compared with the real situation where inputs are not necessarily synchronous. However, it has been shown that L4 neurons can be simultaneously activated under physiological conditions (Petersen and Sakmann, 2001). Different number of inputs (presynaptic neurons) (from four to 40 cells, with an increased step of four) was applied simultaneously at a postsynaptic neuron (resting membrane potential was held at ~−50 mV). For each number of inputs, 50 stimuli were given at an interval of 200 ms, and the EPSPs elicited upon the conductance change were recorded at a postsynaptic cell. First, we compared the threshold number of inputs required to elicit APs at the postsynaptic neuron in both cortices (Fig. 6*A*). Here, threshold was defined as the minimum number of inputs required to induce an AP spike during the entire protocol (50 stimuli). In V1, some postsynaptic neurons did not fire any AP until the highest number of synaptic inputs was applied; in these cases, the highest number plus four was given for the threshold number. As Figure 6*A* shows, the threshold number of S1 connections (13 inputs) was significantly lower than that of V1 connections (28 inputs). Second, the probability of AP firing upon stimulation was plotted against the number of inputs in Figure 6*B*. Clearly, more APs were observed upon the same number of inputs at S1 connections than at V1 ones. Therefore, either the intrinsic membrane properties are different and the S1 neurons fire more easily or the synaptic conductances at S1 induce more firing. To study the effect of the latter, synaptic conductances of S1 and V1 were injected into the same neuron (either S1 or V1) in the next set of experiments. Figure 6, *C* and *D*, show that the S1 conductance induced APs more reliably at both S1 and V1 postsynaptic neurons (for quantification by fitting with a Hill function, see supplemental Fig. 8, available at www.jneurosci.org as supplemental material). These results strongly support the argument that S1 connections are more reliable than V1 connections, due to their synaptic properties.

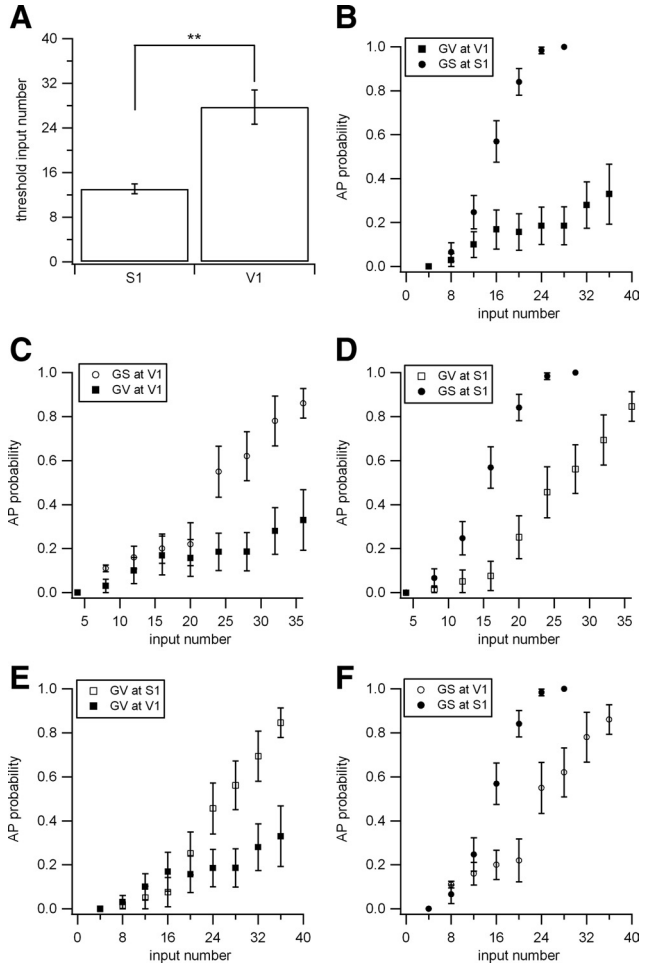

Figure 6. S1 connections induce postsynaptic spikes more than V1 connections. Dynamic clamp was used to examine the consequences of the different synaptic features between the two cortical areas on the postsynaptic AP firing. The synaptic conductances obtained from S1 and V1 are GV and GS, respectively. ***A***, The threshold input number required to elicit APs at a postsynaptic neuron in S1 and V1, when GS and GV were applied to S1 and V1, respectively. The threshold in S1 was significantly lower than that in V1 (*t* test, $p \leq 0.0002$). ***B–F***, The probabilities of firing APs at a postsynaptic neuron upon different input number were plotted. Filled circles represent the AP probability when S1 postsynaptic neurons were stimulated with S1 input parameters (with conductance change measured from S1 connections) ($n = 16–22$ cells; $n = 5$ cells for the data point of 28 inputs). Open circles represent the AP probability when V1 postsynaptic neurons were stimulated with S1 input parameters ($n = 3–9$ cells). Filled squares represent the AP probability when V1 postsynaptic neurons were stimulated with V1 input parameters ($n = 8–16$ cells, $n = 3$ cells for the data point of 40 inputs). Open squares represent the AP probability when S1 postsynaptic neurons were stimulated with V1 input parameters ($n = 7–15$ cells).

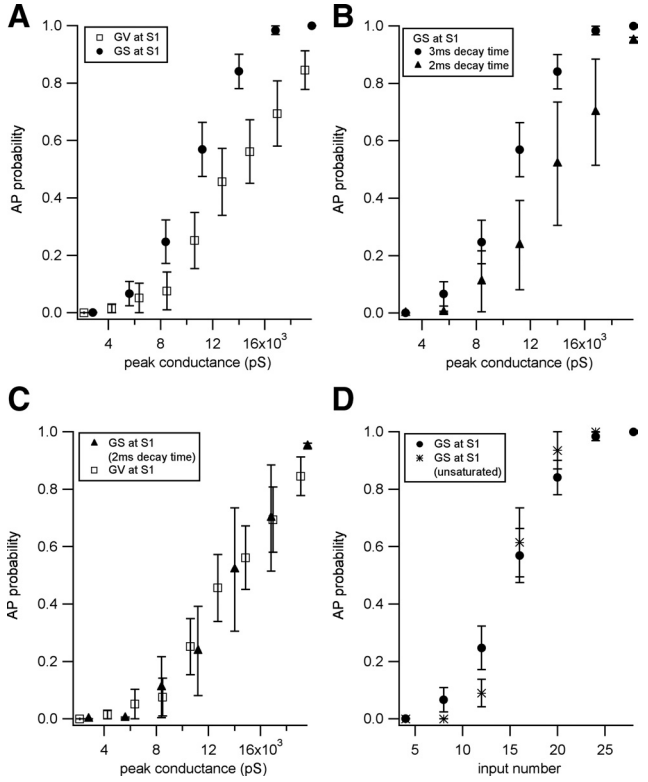

Figure 7. The effects of decay time constant and fluctuation of the postsynaptic responses on the postsynaptic AP firing at the S1 neuron. The same experiment as Figure 6, using dynamic clamp. ***A***, The data are the same as Figure 6 *D*, but the probability of AP firing at the S1 neuron is plotted against the peak amplitude of synaptic conductance, thereby canceling the effect of a difference in the amplitude between GV (synaptic conductance from V1) and GS (synaptic conductance from S1). In this plot, GS induces more firing. When the data were quantified by a Hill function, the GS data could be fitted with $n = 5.6$ and half maximal of 10,410 pS, whereas the GV data could be fitted with $n = 4.4$ and half maximal of 13,674 pS, indicating that the difference is ~30%. The result indicates that either decay time constant of the synaptic conductance (2 vs 3 ms; supplemental information 7, available at www.jneurosci.org as supplemental material) or fluctuation (SD) of the synaptic conductance is responsible for the difference. The same plot at the V1 neuron showed no major difference between GV and GS (data not shown). ***B***, The synaptic decay time constant of 2 or 3 ms was used. Other parameters remained the same as the original GS. The number of synaptic inputs was varied and was applied to the S1 neuron. The 3 ms decay could induce more spikes, indicating that the decay time constant had a consequence on the postsynaptic firing. When the data were fitted by a Hill function, the 3 ms data could be fitted with $n = 5.6$ and half maximal of 10,411 pS, whereas the 2 ms data could be fitted with $n = 5.5$ and half max of 13,769 pS, indicating the rightward shift of the relationship by 30%. Given that GV and GS had a difference in the half maximal of 70% (Fig. 6), ~40% of the difference could be explained by different synaptic decay. ***C***, GS with the decay time constant of 2 ms (the same data as ***B***) and GV (originally the decay time constant of 2 ms) were applied to the S1 neuron. The AP probability is plotted against the peak conductance. The data overlap, suggesting that the GV is less reliable to induce the postsynaptic AP because of faster synaptic decay, in addition to the smaller peak amplitude. ***D***, In this panel, the effect of synaptic fluctuation was tested. Because of postsynaptic receptor saturation, GS fluctuates less than the condition without saturation. In this experiment, in addition to the original GS, the synaptic conductance assuming no receptor saturation was used. This was calculated by using the Kyn data, scaling up by the Kyn blocking efficiency (mean of 760 pS, SD of 200 pS). The two conditions had almost no difference (except a small difference at the low end of the input–output relationship), indicating relatively minor effect of the receptor saturation on the postsynaptic AP firing.

There are three differences in the conductance waveform parameters between S1 and V1: the peak amplitude, decay time constant, and fluctuation (standard deviation). We isolated the effects of decay time constant and fluctuation in Figure 7 by replotting the AP probability against the amplitude of synaptic conductance. Although the AP probability was not significantly different between applying V1 conductance and S1 conductance at the V1 postsynaptic neurons (data not shown), it showed a difference at the S1 postsynaptic neurons (Fig. 7*A*). Furthermore, we found that decreasing the decay time constant from 3 to 2 ms decreased the AP probability in S1 (Fig. 7*B*), which explained ~40% of the total difference shown in Figure 6*D*. On the other side, fluctuation of the amplitudes, which is determined by the transmitter release fluctuation and the postsynaptic receptor saturation, had only a minor effect (Fig. 7*C*,*D*). Therefore, the peak synaptic conductance (determined by MVR and Pr), as well as the synaptic decay (determined postsynaptically), make a difference in the postsynaptic AP firing between S1 and V1.

When Figure 6 panels *B–D* were compared, the differences seem to be more pronounced in Figure 6*B*. In addition, Figure 6,

E and *F*, show that the same conductance parameters (regardless of V1 or S1) elicited higher AP more effectively at the S1 postsynaptic neuron. Therefore, factors other than the synaptic conductance (such as the intrinsic membrane properties) do affect reliable AP firing at the S1 neuron upon presynaptic firing. We quantified the data of Figure 6 with a Hill function (supplemental information 8, available at www.jneurosci.org as supplemental material) and found that contribution of synaptic conductance and intrinsic membrane properties contribute equally to more effective AP firing at S1. One possible source could be the input resistance of the neurons. We measured the input resistance, as shown in supplemental Figure S9 (available at www.jneurosci.org as supplemental material), and found no significant difference between S1 RS neurons and V1 RS neurons (supplemental Fig. S9*C*). Furthermore, the input threshold was not dependent on the input resistance in both cortices (supplemental Fig. S9*A*,*B*). The data show that input resistance does not contribute much to the reliability of the AP firing at the postsynaptic cell. Therefore, the intrinsic membrane properties, other than input resistance at the postsynaptic neuron, are important to make S1 connections more reliable than V1 connections, which remain to be investigated in future studies.

Discussion

We have identified quantal parameters in two primary sensory cortical areas using two independent methods. Pr in V1 neurons was quite heterogeneous compared with S1. Furthermore, we observed MVR in RS–RS connections in L4 in S1, whereas in V1, a single release site can release a single vesicle under physiological conditions. Together with postsynaptic receptor saturation characteristics, the behavior of a synapse in the two cortical regions can be well described. In response to a presynaptic AP, the S1 connections more reliably induce the postsynaptic APs due to the high Pr, MVR, and possibly the synaptic decay and intrinsic membrane properties. During a train of APs, the receptor saturation, in addition to high vesicle replenishment rates, compensates for vesicle pool depletion such that presynaptic APs can cause robust postsynaptic responses.

Multivesicular release at cortical synapses

The theory of release process is classified into two hypotheses. One is the one-release site, one-vesicle hypothesis, which means that at most one vesicle would be released at one release site upon an AP (Korn et al., 1981; Silver et al., 2003), and the other is MVR, which means more than one vesicle can be released at one release site (Tong and Jahr, 1994). In large synapses like the calyx of Held (Taschenberger et al., 2002), climbing fiber in cerebellum (Wadiche and Jahr, 2001) and ribbon synapses (Glowatzki and Fuchs, 2002; Singer et al., 2004; Li et al., 2009) MVR was commonly observed. Multivesicular release was also found at more conventional synapses such as hippocampal Schaffer collateral-CA1 synapses (Oertner et al., 2002). However, at cortical synapses it is suggested that release is constrained to a single vesicle per AP (Buhl et al., 1997; Egger et al., 1999; Feldmeyer et al., 1999; Silver et al., 2003). One study reported MVR at L2/3 neurons in V1 at room temperature (Watanabe et al., 2005), which was in contrast with other reports in S1 (Rozov et al., 2001; Koester and Johnston, 2005). Another recent study suggested that MVR occurred at L5 synapses in S1 (Loebel et al., 2009). Here, our data provide strong evidence in favor of MVR at RS–RS connections of L4 in S1 under physiological conditions based on the differential block of Kyn, which clearly indicates that the local glutamate transient changes during the train. Because synaptic contacts are spatially separated (Feldmeyer et al., 1999), glutamate spillover to the neighboring synapses is highly unlikely. Furthermore, significant receptor saturation was indicated from the variance-mean analysis, which is consistent with MVR. The single vesicle hypothesis was often postulated based on the demonstration that the functional N matched with the anatomical N (Korn et al., 1981; Gulyás et al., 1993; Buhl et al., 1997; Silver et al., 2003; Biró et al., 2005). Although it is definitely informative to make such comparisons, a strong correlation between the two numbers does not necessarily imply that only a single vesicle can be released at each individual release site upon one AP. This only holds true by assuming that the release-ready vesicles are evenly distributed among every anatomical contact. At central synapses, this assumption is not always supported and Pr is rather heterogeneous (Rosenmund et al., 1993; Murthy et al., 1997). Without testing the glutamate concentration at the release site, one cannot conclude that only one vesicle is released at one site upon one AP (Silver et al., 2003). Moreover, the binomial model and variance-mean analysis both require the assumption that postsynaptic receptors are linear indicators of release. If there is receptor saturation, then the assumption would not be satisfied. One might underestimate N in such a scenario. The functional N of L4 connections in S1 (6–8) was twice as many as the anatomical synapse number in rats (3–4) (Feldmeyer et al., 1999), which is consistent with MVR. Therefore, assuming anatomical N as functional N in RS–RS connections in L4 of S1 (Egger et al., 1999) might be misleading. At hippocampal and cerebellar synapses, a synaptic bouton contains a number of docked vesicles (Schikorski and Stevens, 1997; Xu-Friedman et al., 2001). At cortical synapses, the number of docked vesicles per active zone has not been measured precisely. A direct correlation between the number of docked vesicles and the number of releasable vesicles per synapse remains to be found.

In contrast, RS–RS connections of L4 in V1 did not show a differential block by Kyn, indicating a single vesicle release under physiological condition. Since the Pr in V1 is, on average, lower than that in S1, we tested whether those connections could exhibit MVR when the Pr was increased. Surprisingly, differential block by Kyn was observed when TEA was applied, suggesting that a single release site could support release of more than one vesicle per site upon a single AP at high Pr in V1. This argues against the existence of a single vesicle release constraint at least in RS–RS connections. It is important to note that even under high Pr, the differential block was less pronounced compared with S1. This means that apart from the Pr, the synapses at the somatosensory cortex intrinsically favor MVR. Nevertheless, the difference in Pr and degree of postsynaptic receptor saturation distinguishes the same type of connections in two cortical areas from each other. Because of the receptor saturation, S1 connections may be less prone to synaptic plasticity such as long-term potentiation (Egger et al., 1999), whereas the V1 connections are more modifiable upon different stimuli.

Similarities and differences of synapses at two sensory areas and their physiological implication

The connections in V1 show heterogeneous Pr, whereas those in S1 are more homogeneous. There could be several reasons for this disparity. The Ca^{2+} sensor of the release machineries for the two systems could be different. It is possible that the distance between the vesicles and Ca^{2+} channels in V1 connections is more variable than that in S1 connections. The cell morphology in the two cortical regions could be different. The location of synaptic contact in V1 might be more diverse than in S1, or the axon arbor could be wider in V1. Furthermore, the vesicle replen-

ishment rates differ from V1 to S1 neurons. Upon a strong depolarization (depletion pulse), vesicle replenishment rates in S1 were ~3 times faster than those in V1 (T_{rec} in S1, 30 ms; T_{rec} in V1, 100 ms). In contrast, when we fit the depression curve of the train stimulation, the replenishment rates were the same in both cortical regions (T_{rec} of both, 100 ms). During a long depolarization, there is a massive presynaptic Ca^{2+} influx, which most likely speeds up the replenishment process in S1, whereas in V1 this process is saturated during a 50 Hz stimulation. Nevertheless, the vesicle replenishment rate is much faster than retinal bipolar cells (Mennerick and Matthews, 1996) and the calyx of Held (Wu and Borst, 1999) (the order of seconds), and is comparable to mossy fiber and parallel fiber synapses in cerebellum (Saviane and Silver, 2006; Crowley et al., 2007) as well as hair cell synapses (Moser and Beutner, 2000; Griesinger et al., 2005; Li et al., 2009). Since a prolonged depolarization did not release more vesicles compared with an AP train, no reluctant vesicles exist at the L4 synapse (Mennerick and Matthews, 1996; Neher and Sakaba, 2001; Hallermann et al., 2003). Thus, the cortical synapses with a limited number of functional release sites may be able to maintain effective transmission by fast vesicle replenishment together with a high release probability.

The dynamic clamp experiment (Fig. 6) further demonstrates that S1 synaptic conductances can elicit APs more reliably at the postsynaptic neuron. Therefore, the differences in synaptic parameters (high Pr and slower synaptic decay) enable more reliable AP firing at the postsynaptic neuron. To elicit an AP at the postsynaptic site, both S1 and V1 need a convergence of multiple presynaptic inputs (>4) (Fig. 6). This is consistent with the finding that multiple RS neurons can be activated simultaneously within the cortical column under more physiological condition (Petersen and Sakmann, 2000). Because altering the decay time of the simulated synaptic conductance by 1 ms has an effect on spike generation (Fig. 7), the efficacy with which multiple synaptic inputs can elicit postsynaptic spikes would be, in part, determined by the degree of synchrony between those inputs. Although other factors, such as the intrinsic membrane properties (Na^+ channel activation, K^+ channel inactivation, etc.) are equally important for reliable firing, synaptic mechanisms definitely play a major role.

Moreover, if we consider the morphological differences, the RS–RS network of L4 in S1 can integrate signals from various inputs into steady but specific outputs. This is because the neurons form a barrel structure (Feldmeyer et al., 1999; Petersen and Sakmann, 2000) and the intracolumn connection rates are much higher than the intercolumn ones (20%) (Lefort et al., 2009). However, the same network in V1 does not show such strong integration in L4. Connectivity is very low (5%) (Rochefort et al., 2009; our unpublished observation), which makes coupling between neurons highly unreliable. Also, heterogeneous Pr might imply that the postsynaptic neurons integrate various kinds of signals. Thus, we suggest that these differences in structural and physiological properties might correlate to the underlying functional tasks of the respective cortical areas.

References

Abbott LF, Regehr WG (2004) Synaptic computation. Nature 431:796–803.

Abbott LF, Varela JA, Sen K, Nelson SB (1997) Synaptic depression and cortical gain control. Science 275:220–224.

Agmon A, Connors BW (1991) Thalamocortical responses of mouse somatosensory (barrel) cortex in vitro. Neuroscience 41:365–379.

Beierlein M, Gibson JR, Connors BW (2003) Two dynamically distinct inhibitory networks in layer 4 of the neocortex. J Neurophysiol 90:2987–3000.

Biró AA, Holderith NB, Nusser Z (2005) Quantal size is independent of the release probability at hippocampal excitatory synapses. J Neurosci 25:223–232.

Buhl EH, Tamás G, Szilágyi T, Stricker C, Paulsen O, Somogyi P (1997) Effect, number and location of synapses made by single pyramidal cells onto aspiny interneurones of cat visual cortex. J Physiol 500:689–713.

Cook DL, Schwindt PC, Grande LA, Spain WJ (2003) Synaptic depression in the localization of sound. Nature 421:66–70.

Crowley JJ, Carter AG, Regehr WG (2007) Fast vesicle replenishment and rapid recovery from desensitization at a single synaptic release site. J Neurosci 27:5448–5460.

Del Castillo J, Katz B (1954) Quantal components of the end-plate potential. J Physiol 124:560–573.

Diamond JS, Jahr CE (1995) Asynchronous release of synaptic vesicles determines the time course of the AMPA receptor-mediated EPSC. Neuron 15:1097–1107.

Diamond JS, Jahr CE (1997) Transporters buffer synaptically released glutamate on a submillisecond time scale. J Neurosci 17:4672–4687.

Dittman JS, Regehr WG (1998) Calcium dependence and recovery kinetics of presynaptic depression at the climbing fiber to Purkinje cell synapse. J Neurosci 18:6147–6162.

Dobrunz LE, Stevens CF (1997) Heterogeneity of release probability, facilitation, and depletion at central synapses. Neuron 18:995–1008.

Egger V, Feldmeyer D, Sakmann B (1999) Coincidence detection and changes of synaptic efficacy in spiny stellate neurons in rat barrel cortex. Nat Neurosci 2:1098–1105.

Feldmeyer D, Egger V, Lubke J, Sakmann B (1999) Reliable synaptic connections between pairs of excitatory layer 4 neurones within a single 'barrel' of developing rat somatosensory cortex. J Physiol 521:169–190.

Foster KA, Regehr WG (2004) Variance-mean analysis in the presence of a rapid antagonist indicates vesicle depletion underlies depression at the climbing fiber synapse. Neuron 43:119–131.

Foster KA, Kreitzer AC, Regehr WG (2002) Interaction of postsynaptic receptor saturation with presynaptic mechanisms produces a reliable synapse. Neuron 36:1115–1126.

Glowatzki E, Fuchs PA (2002) Transmitter release at the hair cell ribbon synapse. Nat Neurosci 5:147–154.

Griesinger CB, Richards CD, Ashmore JF (2005) Fast vesicle replenishment allows indefatigable signalling at the first auditory synapse. Nature 435:212–215.

Gulyás AI, Miles R, Sík A, Tóth K, Tamamaki N, Freund TF (1993) Hippocampal pyramidal cells excite inhibitory neurons through a single release site. Nature 366:683–687.

Gupta A, Wang Y, Markram H (2000) Organizing principles for a diversity of GABAergic interneurons and synapses in the neocortex. Science 287:273–278.

Hallermann S, Pawlu C, Jonas P, Heckmann M (2003) A large pool of releasable vesicles in a cortical glutamatergic synapse. Proc Natl Acad Sci U S A 100:8975–8980.

Harrison J, Jahr CE (2003) Receptor occupancy limits synaptic depression at climbing fiber synapses. J Neurosci 23:377–383.

Hosoi N, Sakaba T, Neher E (2007) Quantitative analysis of calcium-dependent vesicle recruitment and its functional role at the calyx of Held synapse. J Neurosci 27:14286–14298.

Isaacson JS, Walmsley B (1995) Counting quanta: direct measurements of transmitter release at a central synapse. Neuron 15:875–884.

Katz B, Miledi R (1965) The measurement of synaptic delay, and the time course of acetylcholine release at the neuromuscular junction. Proc R Soc Lond B Biol Sci 161:483–495.

Katz B, Miledi R (1967) The release of acetylcholine from nerve endings by graded electric pulses. Proc R Soc Lond B Biol Sci 167:23–38.

Koester HJ, Johnston D (2005) Target cell-dependent normalization of transmitter release at neocortical synapses. Science 308:863–866.

Korn H, Triller A, Mallet A, Faber DS (1981) Fluctuating responses at a central synapse: n of binomial fit predicts number of stained presynaptic boutons. Science 213:898–901.

Lefort S, Tomm C, Floyd Sarria JC, Petersen CC (2009) The excitatory neuronal network of the C2 barrel column in mouse primary somatosensory cortex. Neuron 61:301–316.

Li GL, Keen E, Andor-Ardó D, Hudspeth AJ, von Gersdorff H (2009) The unitary event underlying multiquantal EPSCs at a hair cell's ribbon synapse. J Neurosci 29:7558–7568.

Loebel A, Silberberg G, Helbig D, Markram H, Tsodyks M, Richardson MJ (2009) Multiquantal release underlies the distribution of synaptic efficacies in the neocortex. Front Comput Neurosci 3:27.

Lübke J, Egger V, Sakmann B, Feldmeyer D (2000) Columnar organization of dendrites and axons of single and synaptically coupled excitatory spiny neurons in layer 4 of the rat barrel cortex. J Neurosci 20:5300–5311.

Mennerick S, Matthews G (1996) Ultrafast exocytosis elicited by calcium current in synaptic terminals of retinal bipolar neurons. Neuron 17:1241–1249.

Meyer AC, Neher E, Schneggenburger R (2001) Estimation of quantal size and number of functional active zones at the calyx of held synapse by nonstationary EPSC variance analysis. J Neurosci 21:7889–7900.

Moser T, Beutner D (2000) Kinetics of exocytosis and endocytosis at the cochlear inner hair cell afferent synapse of the mouse. Proc Natl Acad Sci U S A 97:883–888.

Murphy GJ, Glickfeld LL, Balsen Z, Isaacson JS (2004) Sensory neuron signaling to the brain: properties of transmitter release from olfactory nerve terminals. J Neurosci 24:3023–3030.

Murthy VN, Sejnowski TJ, Stevens CF (1997) Heterogeneous release properties of visualized individual hippocampal synapses. Neuron 18:599–612.

Neher E, Sakaba T (2001) Combining deconvolution and noise analysis for the estimation of transmitter release rates at the calyx of held. J Neurosci 21:444–461.

Oertner TG, Sabatini BL, Nimchinsky EA, Svoboda K (2002) Facilitation at single synapses probed with optical quantal analysis. Nat Neurosci 5:657–664.

Petersen CC (2002) Short-term dynamics of synaptic transmission within the excitatory neuronal network of rat layer 4 barrel cortex. J Neurophysiol 87:2904–2914.

Petersen CC, Sakmann B (2000) The excitatory neuronal network of rat layer 4 barrel cortex. J Neurosci 20:7579–7586.

Petersen CC, Sakmann B (2001) Functionally independent columns of rat somatosensory barrel cortex revealed with voltage-sensitive dye imaging. J Neurosci 21:8435–8446.

Prinz AA, Abbott LF, Marder E (2004) The dynamic clamp comes of age. Trends Neurosci 27:218–224.

Rochefort NL, Garaschuk O, Milos RI, Narushima M, Marandi N, Pichler B, Kovalchuk Y, Konnerth A (2009) Sparsification of neuronal activity in the visual cortex at eye-opening. Proc Natl Acad Sci U S A 106:15049–15054.

Rosenmund C, Clements JD, Westbrook GL (1993) Nonuniform probability of glutamate release at a hippocampal synapse. Science 262:754–757.

Rozov A, Burnashev N, Sakmann B, Neher E (2001) Transmitter release modulation by intracellular Ca^{2+} buffers in facilitating and depressing nerve terminals of pyramidal cells in layer 2/3 of the rat neocortex indicates a target cell-specific difference in presynaptic calcium dynamics. J Physiol 531:807–826.

Saviane C, Silver RA (2006) Errors in the estimation of the variance: implications for multiple-probability fluctuation analysis. J Neurosci Methods 153:250–260.

Scheuss V, Neher E (2001) Estimating synaptic parameters from mean, variance, and covariance in trains of synaptic responses. Biophys J 81:1970–1989.

Schikorski T, Stevens CF (1997) Quantitaive ultrastructural analysis of hippocampal excitatory synapses. J Neurosci 17:5858–5867.

Silver RA (2003) Estimation of nonuniform quantal parameters with multiple-probability fluctuation analysis: theory, application and limitations. J Neurosci Methods 130:127–141.

Silver RA, Lubke J, Sakmann B, Feldmeyer D (2003) High-probability uniquantal transmission at excitatory synapses in barrel cortex. Science 302:1981–1984.

Singer JH, Lassová L, Vardi N, Diamond JS (2004) Coordinated multivesicular release at a mammalian ribbon synapse. Nat Neurosci 7:826–833.

Stern P, Edwards FA, Sakmann B (1992) Fast and slow components of unitary EPSCs on stellate cells elicited by focal stimulation in slices of rat visual cortex. J Physiol 449:247–278.

Stevens CF, Wang Y (1995) Facilitation and depression at single central synapses. Neuron 14:795–802.

Taschenberger H, Leão RM, Rowland KC, Spirou GA, von Gersdorff H (2002) Optimizing synaptic architecture and efficiency for high-frequency transmission. Neuron 36:1127–1143.

Thomson AM (2000) Facilitation, augmentation and potentiation at central synapses. Trends Neurosci 23:305–312.

Tong G, Jahr CE (1994) Multivesicular release from excitatory synapses of cultured hippocampal neurons. Neuron 12:51–59.

Trussell LO, Zhang S, Raman IM (1993) Desensitization of AMPA receptors upon multiquantal neurotransmitter release. Neuron 10:1185–1196.

Van der Kloot W (1988) The kinetics of quantal releases during end-plate currents at the frog neuromuscular junction. J Physiol 402:605–626.

Vere-Jones D (1966) Simple stochastic models for the release of quanta of transmitter from a nerve terminal. Aust J Stat 8:53–63.

Wadiche JI, Jahr CE (2001) Multivesicular release at climbing fiber-Purkinje cell synapses. Neuron 32:301–313.

Wang LY, Kaczmarek LK (1998) High-frequency firing helps replenish the readily releasable pool of synaptic vesicles. Nature 394:384–388.

Watanabe J, Rozov A, Wollmuth LP (2005) Target-specific regulation of synaptic amplitudes in the neocortex. J Neurosci 25:1024–1033.

Wu LG, Borst JGG (1999) The reduced release probability of releasable vesicles during recovery from short-term depression. Neuron 23:821–832.

Xu-Friedman MA, Harris KM, Regehr WG (2001) Three-dimensional comparison of ultrastructural characteristics at depressing and facilitating synapses onto cerebellar Purkinje cells. J Neurosci 17:6666–6672.

Zucker RS, Regehr WG (2002) Short-term synaptic plasticity. Annu Rev Physiol 64:355–405.